Author/s:
Tyshchenko, I;Lévy, S;Bartlett, JJ;Tahayori, B;Blunck, Y;Sava, TV;Chow, K;Liebig, P;Glarin, R;Johnston, LA

Title:
In vivo evaluation of population-specific inversion pulses in parallel transmission

Date:
2025-11-01

Citation:
Tyshchenko, I., Lévy, S., Bartlett, J. J., Tahayori, B., Blunck, Y., Sava, T. V., Chow, K., Liebig, P., Glarin, R. & Johnston, L. A. (2025). In vivo evaluation of population-specific inversion pulses in parallel transmission. Magnetic Resonance in Medicine, 94 (5), pp.1878-1888. https://doi.org/10.1002/mrm.30593.

Persistent Link:
https://hdl.handle.net/11343/362573

Received: 29 October 2024 | Revised: 15 May 2025 | Accepted: 16 May 2025

DOI: 10.1002/mrm.30593

RESEARCH ARTICLE

Magnetic Resonance in Medicine

In vivo evaluation of population-specific inversion pulses in parallel transmission

Igor Tyshchenko[1,2] | **Simon Lévy**[3] | **Joseph J. Bartlett**[1,2,4] | **Bahman Tahayori**[5] | **Yasmin Blunck**[1,2] | **Tudor V. Sava**[2] | **Kelvin Chow**[6] | **Patrick Liebig**[7] | **Rebecca Glarin**[2] | **Leigh A. Johnston**[1,2]

[1]Department of Biomedical Engineering and Graeme Clark Institute, The University of Melbourne, Victoria, Australia

[2]Melbourne Brain Centre Imaging Unit, The University of Melbourne, Victoria, Australia

[3]MR Research Collaborations, Siemens Healthcare Pty Ltd, Victoria, Australia

[4]School of Computer Science, University of Birmingham, Birmingham, UK

[5]The Florey Institute of Neuroscience and Mental Health, Victoria, Australia

[6]Cardiovascular MR R&D, Siemens Healthcare GmbH, Calgary, Canada

[7]Siemens Healthcare GmbH, Erlangen, Germany

Correspondence
Igor Tyshchenko, Melbourne Brain Centre Imaging Unit, The University of Melbourne, Victoria, Australia.
Email: ityshchenko@student.unimelb.edu.au

Abstract

Purpose: The aim of the study was to conduct in vivo evaluation of population-specific pulses in the context of the MP2RAGE sequence for brain imaging at 7T.

Methods: Five clusters were identified in a cohort of 39 volunteers. One cluster centered around the average head shape and position, whereas four others were located toward the extremes of the population distribution. Additionally, the one-size-fits-all solution was considered, using a standard universal pulse (UP) approach. Head shapes were characterized using lateral head breadth (HB), anterior–posterior head length (HL), and Y-shift metrics. For each group, a 5kT-points universal inversion pulse was computed and evaluated on four new test anatomies. A Python pipeline was integrated into the image reconstruction routine, using localizer scans to classify head shapes and positions. The pipeline selected one of five precomputed population-specific pulses or defaulted to the generic UP without extending scan time.

Results: The pipeline accurately classified head shapes and selected suitable pulses, enhancing the contrast of MP2RAGE images. Population-specific pulses helped mitigate some of the performance loss associated with using a one-size-fits-all UP, bringing performance closer to that of fully tailored solutions. This approach was particularly beneficial for individuals with smaller head sizes. However, the performance was worse in larger, more challenging head shapes.

Conclusion: The novel head clustering and pulse selection pipeline facilitates the implementation of population-specific pulses in clinical practice by allowing pulse selection tailored to each head shape and position without increasing scan time.

KEYWORDS

MRI, UHF, parallel transmission, universal pulse, RF pulse design, k_T-points

1 | INTRODUCTION

Ultra-high field (UHF) MRI encounters significant obstacles due to the radiofrequency (RF) wavelengths being comparable to the size of the human head. This similarity in scale leads to complex wave interactions, resulting in nonuniform B_1^+ fields that vary from subject to subject during brain imaging.[1–3] Clinically, the use of UHF MRI has been restricted by spatially varying contrast arising from the inhomogeneous B_+^1 fields, susceptibility artifacts, and unwanted heating from high specific absorption rate (SAR).[4–6]

One of the most effective strategies for mitigating B_1^+ inhomogeneity involves the use of adiabatic pulses.[7] In these pulses, both the amplitude and frequency of the RF field are modulated, resulting in waveforms that are robust against off-resonance effects. While adiabatic pulses effectively address transmit field inhomogeneities, they generally have longer durations, demand higher RF amplitudes, and are associated with increased SAR.

Parallel transmission (pTx) has demonstrated potential in mitigating both B_+^1 inhomogeneities and SAR issues. Achieving optimal performance with pTx requires tailoring the RF pulses to each subject's individual B_0 and B_+^1 distributions. However, this optimization process is unrealistic in clinical settings due to the lengthy process required to acquire field maps and design pulses.[8,9]

To overcome time limitations, alternative calibration-free universal pulses (UP)[10,11] and preoptimized pulses with a brief optimization step such as standardized universal pulses (SUP)[12] and fast online-customized (FOCUS) pulses[13,14] have been actively explored recently. Despite their potential, these approaches still require the acquisition of B_1^+ and B_0 maps and extra optimization, which adds to the overall scan time.

In our previous work, we demonstrated through electromagnetic simulations of a typical 8-channel head coil array that designing pulses for subpopulations with less variation in head shape and position may lead to performance gains at 7T.[15] The most significant B_+^1 improvements were predicted to be in the challenging head shapes at the extremes of the population distribution. Specifically, this approach involved creating distinct population-specific solutions for different subsets of the distribution. By dividing the entire population into subgroups based on similar anatomical shapes and positions, pulses could be designed with reduced anatomical variability.

In this study, our objective was to develop a practical solution for population-specific pulse design and application that optimally balances inversion homogeneity and energy deposition, as compared to standard UPs. To achieve this, we designed, implemented, and tested an automated online image-processing pipeline for head shape clustering and pulse selection. The pipeline was integrated into the standard image reconstruction workflow and accurately classified head shapes while selecting appropriate pulses, enhancing the contrast of MP2RAGE images. This novel pipeline facilitates the population-specific approach by enabling pulse selection tailored to each head shape and position without increasing scan time. Consequently, it supports more personalized and efficient ultra-high field MRI, laying the groundwork for future integration into clinical practice.

2 | METHODS

2.1 | Head measurement

Consistent with our prior studies,[15] three head shape parameters were selected for analysis: lateral head breadth (HB), anterior–posterior head length (HL), and the Y-shift. These measurements were obtained from a localizer scan using an automated Python script.

A reference anatomy was used for the measurement process, with the target slice of interest aligned along the anterior commissure—posterior commissure (AC-PC) line, orthogonal to the sagittal plane. The reference anatomy was registered to the participant's anatomy for each new participant using an affine transformation implemented via the ANTsPy library.[27] The same transformation was applied to the reference slice, allowing us to interpolate the participant's localizer to identify the corresponding slice of interest. This target slice was then subjected to thresholding, after which the HL and HB were determined as the major and minor axis lengths of an ellipse with identical normalized second central moments to the thresholded region. The Y-shift was calculated as the distance between the isocenter and this region's center of mass. To assess measurement variability, a total of 20 automated head measurements were performed for each anatomy.

2.2 | Head anatomies and subpopulations

The dataset of 39 head anatomies, characterized by mean $\mu_{HB,HL,Y} = \{160.32, 201.73, 10.78\}$ mm and standard deviation $\sigma_{HB,HL,Y} = \{6.25, 9.16, 3.23\}$ mm, was partitioned into five clusters (Figure 1). The first cluster (C1) comprised ten anatomies centered around the mean value. The second (C2) and third (C3) clusters each included the five anatomies furthest from the mean on opposite sides of the population distribution. Similarly, the fourth (C4) and fifth

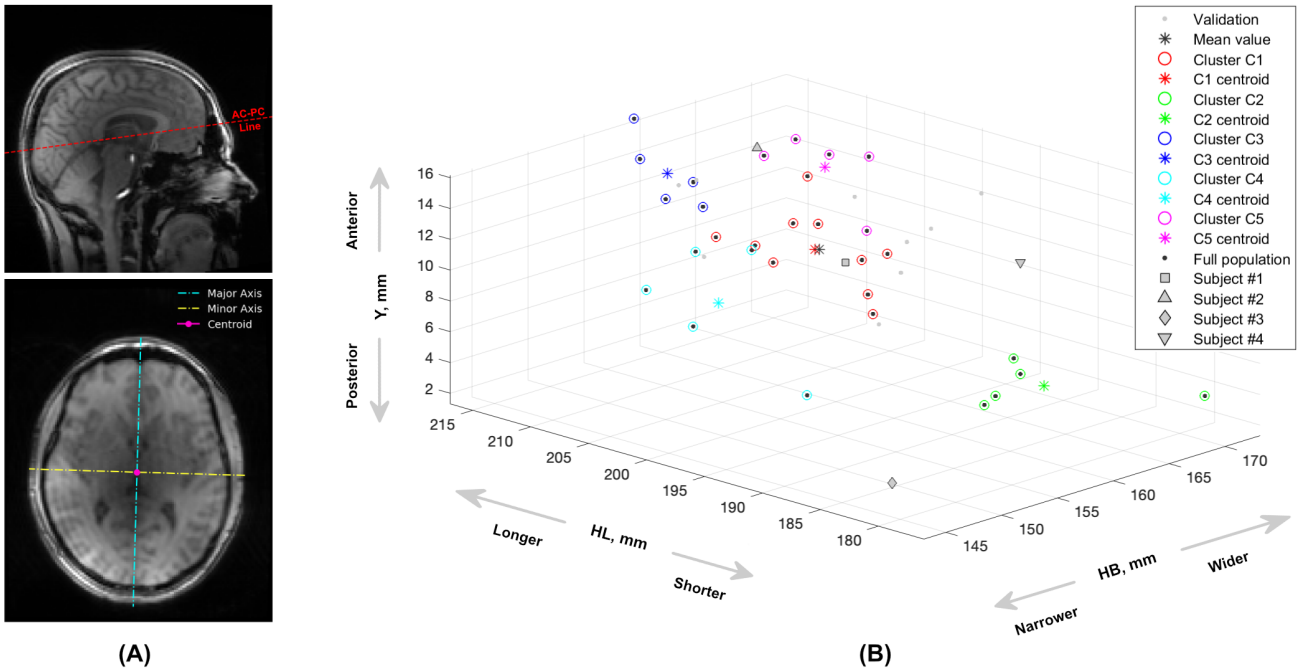

FIGURE 1 (A) Slice of interest through the anterior commissure—posterior commissure (AC-PC) line orthogonal to the sagittal plane. The head shapes were characterized by three parameters: lateral head breadth (HB), anterior–posterior head length (HL), and Y-shift (displacement along the anterior–posterior axis). The HL and HB were measured as the major and minor axis lengths of the ellipse with the same normalized second central moments as the thresholded slice of interest. The Y-shift was calculated as the distance between that region's center of mass and the coil's isocenter. (B) Scatter plot illustrating the head anatomies considered in this study as measured by the automated pipeline. Five clusters are shown, including C1—red, C2—green, C3—blue, C4—cyan and C5—magenta. The set of anatomies, referred to as the "full population", was utilized to design a generic one-size-fits-all UP. Additionally, the nine anatomies used to evaluate the performance of the clustering algorithm and three test subjects used for *in vivo* performance evaluation are shown.

(C5) clusters comprised the next five anatomies closest to the opposite extremes among the remaining data. Finally, all five clusters were combined to represent the full population. Detailed demographics of the volunteers and cluster compositions are provided in Table S1.

After identifying the head parameters, the clustering was performed by calculating the Euclidean distance to all cluster centroids listed in Table 1. Each cluster had an acceptable maximum distance threshold set to 7 mm. The clustering algorithm selected the cluster with the shortest distance to its centroid within this maximum threshold. The algorithm defaulted to the generic UP if all distances exceeded the threshold. It was possible to specify a custom threshold per cluster, allowing clusters of different sizes to be defined.

2.3 | Pulse design

A nonselective 5kT-points[17] inversion pulse was computed for each cluster. Specifically, a constrained magnitude least squares optimization problem with the target flip angle $\theta = \pi$ was solved[18–20]

$$\{\hat{\mathbf{x}}, \hat{\mathbf{k}}\} = \underset{\mathbf{x},\mathbf{k}}{\operatorname{argmin}} \|\mathcal{B}(\mathbf{x}, \mathbf{k}) - \pi\|_2,$$
$$\mathbf{x} \in \mathbb{C}^{N_c \times N_{kT}}, \quad \mathbf{k} \in \mathbb{R}^{3N_{kT}}, \tag{1}$$

where $\mathbf{x}$ is the concatenation of the $N_c \times N_{kT}$ RF complex amplitudes, $\mathbf{k}$ denotes the concatenation of kT-points coordinates along each axis (k_x, k_y, k_z) and $\mathcal{B}$ is the Bloch integration operator that returns flip angles for voxels within the brain region.

Each subpulse in the solution had a rectangular shape and was 500 μs long, while the gradient blips had a duration of 200 μs. The optimization was performed subject to strict local specific energy dose ($\mathrm{SED}_{\max} = 30$ J/kg) constraints as well as voltage amplitude ($V_{\max} = 170$ V), gradient amplitude ($G_{\max} = 70$ mT/m), and gradient slew rate ($\mathrm{SR}_{\max} = 200$ mT/m/ms) limits.

The optimization (1) was performed within a brain mask obtained from a localizer scan using the brain extraction tool included in the FSL[21] (FMRIB, Oxford, UK) software library. The same library was utilized to resample the mask to match the resolution of B_1^+ and B_0 maps. The 5kT-points inversion pulse design involved the following steps:

TABLE 1 Cluster means and overall mean values for lateral head breadth (HB), anterior–posterior head length (HL), and Y-shift metrics.

	HB, mm	HL, mm	Y, mm
Full	159.88	201.76	10.52
C1	160.25	202.02	10.73
C2	162.96	184.93	4.92
C3	158.72	213.31	13.58
C4	148.87	199.39	10.35
C5	168.22	208.86	12.79

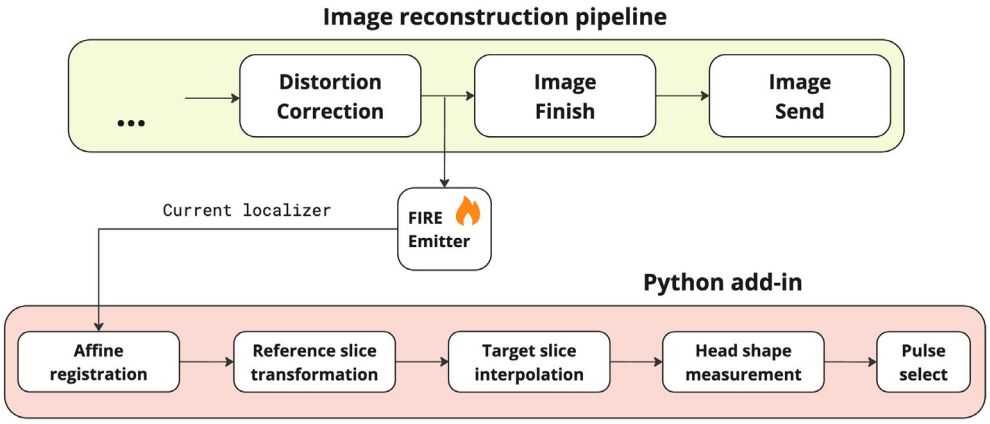

FIGURE 2 A system diagram illustrating the automated head measurement and clustering add-in integrated into the primary image reconstruction pipeline.

1. Two initial sets of RF complex amplitudes were calculated using the 150 V and 140 V circularly polarized (CP) pulses as starting cases for each of the subpulses in the train. Using the active-set MATLAB algorithm (Mathworks, Natick, MA) the RF amplitudes were optimized following equation (1). During this step, the gradients remained zero, and the SED_{max} allowance was set at 30 J/kg. The highest performing solution out of those two sets was selected for the subsequent step;
2. 20 k-space trajectories were generated with kT points coordinates k_i randomly selected from a uniform [−8,8] m^{-1} distribution. Importantly, these initial trajectories remained the same across all populations to reduce the effect of the randomness in the k-space sampling;
3. Using the active-set MATLAB algorithm, both the RF complex amplitudes and the k-space trajectory were optimized simultaneously, producing 20 potential 5kT-points pulses;
4. The solution with the lowest cost function (1) was kept as final.

2.4 | Scanner implementation

The automated Python pipeline was deployed on the MAGNETOM 7T Plus MRI scanner (Siemens Healthineers, Forchheim, Germany), utilizing the Framework for Image Reconstruction Environments (FIRE) recently introduced by the manufacturer.[22] FIRE provides a platform for custom image reconstruction and analysis programs to operate on the scanner's back-end. It interacts using the magnetic resonance data (MRD) format and can transmit raw or reconstructed image data from various stages of the reconstruction process.

For head measurements, the image data was extracted from the reconstruction pipeline by inserting an image emitter immediately after the distortion correction module (Figure 2). Image reconstruction was complete at this stage, allowing us to run any necessary post-processing. While FIRE allows for processed data to be reintegrated into the original pipeline, this functionality was not utilized in our case, as the actual image contrast was not manipulated.

2.5 | Data acquisition and analysis

A cohort of 39 volunteers was scanned using a Nova 8Tx/32Rx head coil (Nova Medical, Wilmington, MA). The imaging protocol included a localizer with voxel size 1.6 × 1.625 × 1.625 mm^3, as well as B_0 and channel-specific B_+^1 mapping sequences,[23,24] provided by the vendor to obtain the requisite data for pulse design.

TABLE 2 The distances to the cluster centroids calculated using the automated pipeline and the Euclidean distance metric.

	C1, mm	C2, mm	C3, mm	C4, mm	C5, mm
Subject #1	**6.85**	11.90	18.29	14.35	14.58
Subject #2	11.71	28.67	6.81	21.11	**4.04**
Subject #3	21.44	**13.35**	31.47	16.50	31.60
Subject #4	15.34	**7.82**	26.66	18.94	22.42

The custom inversion pulses were incorporated into the magnetization-prepared 2 rapid acquisition gradient echo (MP2RAGE) research application sequence.[25] The sequence was executed with the following parameters: TR/TE/TI1/TI2 = 5000/2.04/700/2700 ms, FA1/FA2 = 4/5 deg, FOV = $240 \times 240 \times 154$ mm^3, voxel size = $0.75 \times 0.75 \times 0.75$ mm^3, generalized autocalibrating partially parallel acquisitions (GRAPPA) acceleration factor = 4, and TA = 7:02 min.

The performance of the designed pulses was evaluated *in vivo* on four test subjects who were not part of the original cohort. Following a similar head measurement procedure based on the localizer scan (Table 2), subjects #1 and #2 were classified as C1 and C5, respectively. The third volunteer #3 was equivocally positioned between C2 and C4 was therefore classified as full population. However, due to the proximity to C2, subject #3 was also scanned with that pulse. Subject #4 was classified as C2 and had an abnormally high Y-shift due to large hair volume in the coil. The anatomical classification was performed using the automated pipeline by calculating the Euclidean distance to the centroid of each cluster.

For comparative analysis, each subject was also scanned with the same sequence using a 12.8 ms long hyperbolic secant 4 (HS4) adiabatic inversion pulse, with all other parameters kept constant; this scan is referred to hereafter as HS4-MP2RAGE. Due to time constraints and the computationally intensive nature of our pulse design method, *in vivo* data for the tailored pulses were not acquired.

All MP2RAGE UNI-DEN images were bias-field corrected and registered by rigid transformation to the reference HS4-MP2RAGE using ANTs[26,27] (University of Pennsylvania, Philadelphia, PA) software package. Subsequently, brain masks were obtained using FastSurfer.[28] The relative difference maps within the brain mask were calculated based on the registered T1 maps to quantify the discrepancy between the T1 values and the reference HS4-MP2RAGE. Those maps were generated from two sets of images acquired at different inversion times, aiming to minimize the influence of the B_1^+ inhomogeneity. Any imperfections in the inversion pulse performance would be reflected in the quantitative T1 maps. The comparison was done in four slices that captured the most challenging parts in the temporal lobes and around the sinuses. The slices included a midsagittal slice, left and right sagittal slices capturing the temporal poles, as well as an axial slice through the inferior frontal lobe close to the sinuses.

3 | RESULTS

3.1 | Measurement accuracy

The accuracy of the head measurement was evaluated by running the algorithm 20 times for each of the 39 subjects, accounting for its stochastic nature due to image registration variability. The results showed a standard deviation of less than 0.3 mm (Figure 3A) and a spread of values within 1 mm (Figure 3B) for each measurement set. The automatically identified slices of interest for all 39 subjects aligned well with the AC-PC line. A visualization illustrating the intersection of the midsagittal plane with the target slice identified by the automated measurement pipeline is provided in Figure S1.

3.2 | Performance evaluation

Analysis of the predicted normalized root mean square error (NRMSE) values for the target longitudinal magnetization profile after inversion revealed a clear trend: performance deteriorated for both the adiabatic (Figure 4A) and tailored pulses (Figure 4B) as head shape size increased. As anticipated, the adiabatic inversion yielded the best overall performance outperforming tailored solutions and UP by 34% and 51%, respectively (Table 3). A similar trend was noted with the one-size-fits-all, full population UP approach (Figure 4C). Although this method achieved relatively uniform inversion homogeneity across various head sizes and positions, a discernible decline in performance was still evident for larger head shapes.

In contrast, when using population-specific pulses, cluster C1 (corresponding to the average head shape) displayed performance most similar to that of the full population (Figure 4D). Its mean and maximum NRMSE

FIGURE 3 Accuracy of the automated pipeline measured by (A) the standard deviation across 20 runs and (B) the range between the highest and lowest measurements.

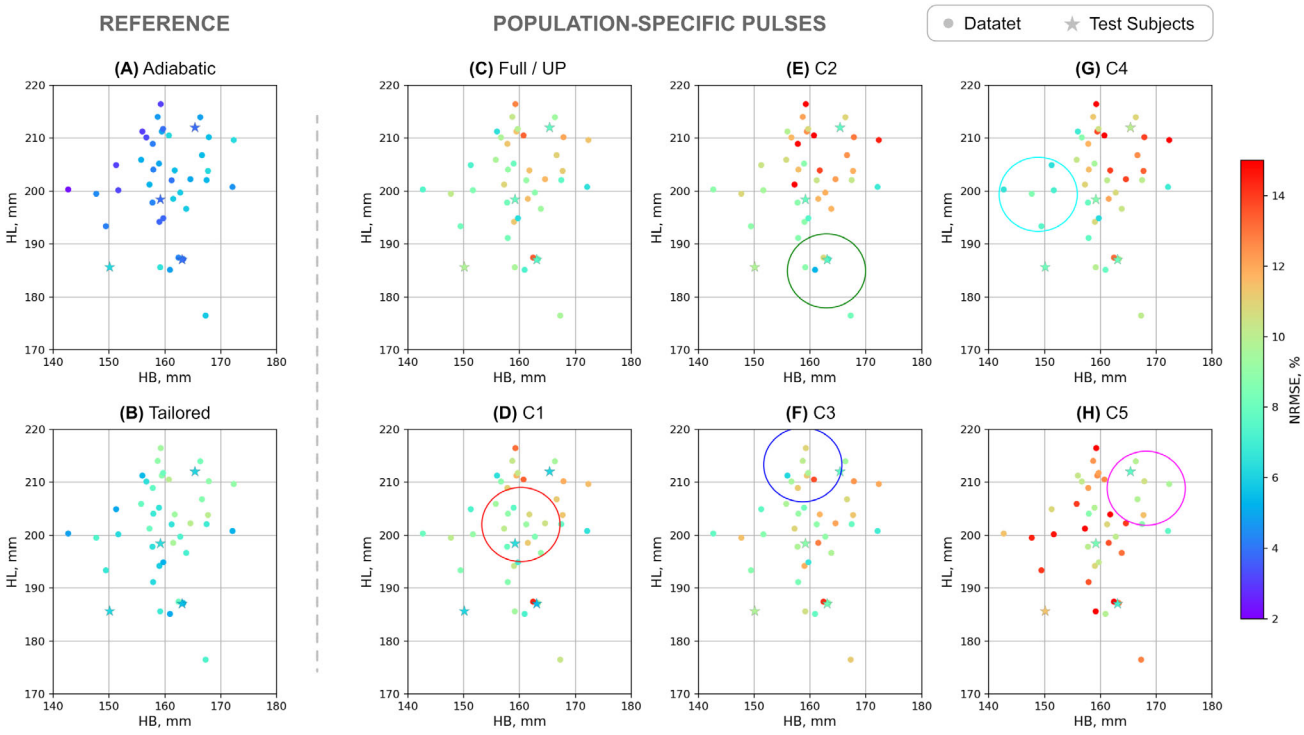

FIGURE 4 Scatter plot of normalized root mean square errors (NRMSE) of the target longitudinal magnetization profile within the brain mask after inversion. The performance of HS4 adiabatic pulse (A) and tailored pulses (B) is compared to that of generic full-population UP (C), and population-specific pulses C1-C5 (D-H) are applied. Colored circles highlight cluster locations and threshold levels used in automated pulse selection; stars indicate test subjects. The Y-axis (third dimension) was flattened for simplicity.

TABLE 3 Performance of HS4 adiabatic inversion, tailored pulses and UP within the dataset.

NRMSE (%)	Min	Mean	Max
HS4	2.29	4.86	6.34
Tailored	4.86	7.38	9.67
UP	6.52	10.02	13.47

TABLE 4 Performance of population-specific pulses C1–C5 within their respective clusters. Values in parentheses indicate performance across the full dataset.

NRMSE (%)	Min	Mean	Max
C1	7.65 (6.43)	9.42 (9.68)	11.20 (14.41)
C2	5.26 (5.26)	8.08 (10.93)	10.77 (17.46)
C3	6.17 (6.17)	9.61 (9.97)	11.25 (14.24)
C4	6.49 (6.24)	7.26 (10.55)	8.56 (16.34)
C5	9.64 (7.73)	10.26 (12.07)	11.45 (17.84)

within the dataset were comparable to those achieved using the UP approach (Table 4). More pronounced performance differences were observed in clusters C2 through C5, which represent the extreme ends of the population distribution (Figure 4E–H). Specifically, the subpopulations with smaller head shapes in clusters C2 (Figure 4E) and C4 (Figure 4G) approximated the performance of the tailored pulses in their respective regions, while a marked decline was observed in the complementary segments of the distribution. Notably, cluster C5 (designed for larger head shapes) demonstrated the poorest overall performance. Furthermore, clusters C2 through C5 showed significant discrepancies between their average and maximum NRMSE values within the cluster and their performance across the full dataset (Table 4).

A visual analysis of MP2RAGE UNI-DEN (uniform denoised) scans indicated that the population-specific pulse resulted in modest contrast improvements around the sinues (as highlighted by red arrows) for Subject #1, categorized as C1 (Figure 5A). In contrast, Subject #2, identified as having the largest head morphology among the test subjects, showed performance deterioration with signs of signal hyperintensity in the midbrain (Figure 5B).

The most pronounced performance enhancements were observed in Subjects #3 and #4 (Figure 5C,D), both characterized by smaller head shapes. Although Subject #3 was automatically classified as full population, applying the C2 pulse closest to it resulted in significant contrast improvements, particularly in recovering signal hyperintensity around the sinuses. A comparable performance improvement was noted in Subject #4, where the majority of contrast around the sinuses and in the left temporal lobe were effectively recovered.

Quantitative analysis of T1 values against gold standard adiabatic inversion revealed that Subject #1 exhibited a slight improvement of 3% in NRMSE after applying the subpopulation pulse (Figure 6A). Conversely, Subject #2 experienced a significant performance deterioration of 52% (Figure 6B). The most notable performance gains were recorded in Subjects #3 and #4, with improvements of 21% and 11%, respectively (Figure 6C,D).

4 | DISCUSSION

This scanner implementation demonstrated that population-specific pulses could be a viable and efficient strategy for integrating them into a clinical routine without requiring additional time to acquire field maps or perform additional optimization. Simulated results and visual comparison of anatomical scans confirmed that the performance of a one-size-fits-all solution could be improved toward smaller head shapes.

Our findings suggest that population-specific pulses can recover some of the NRMSE loss incurred when a one-size-fits-all UP is used, bringing performance closer to that of fully tailored solutions. Smaller head shapes, characterized by less prominent field heterogeneities, benefit the most from this approach. Specifically, Subjects #3 and #4, both characterized by smaller head sizes, demonstrated substantial performance improvements of up to 21%. Larger head shapes remain challenging due to more pronounced field heterogeneities and an increased imaging volume that must be considered. To mitigate the impact of susceptibility-induced artifacts, extended datasets in conjunction with more accurate field mapping

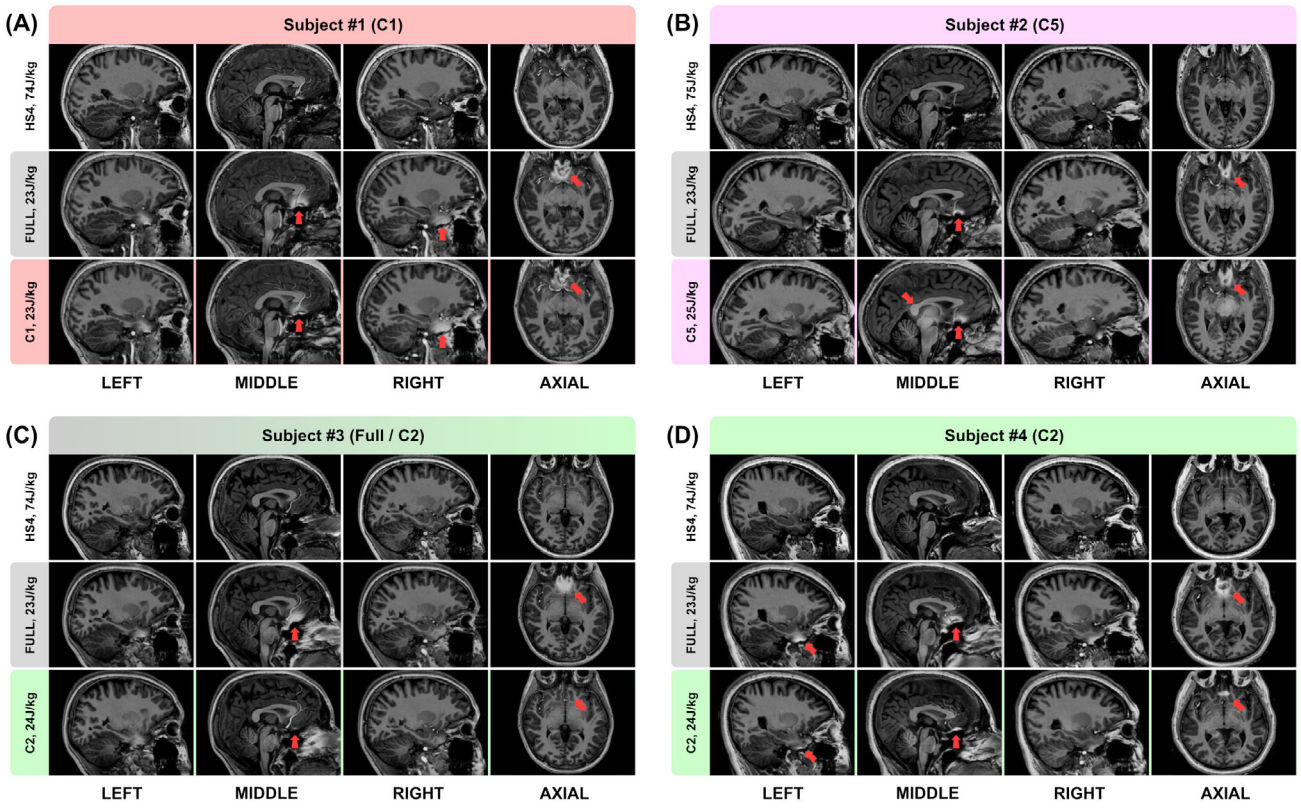

FIGURE 5 Performance of inversion pulses in MP2RAGE UNI-DEN images for subjects #1-4 (A-D). "N, M J/kg" indicates a pulse designed for cluster N with specific energy deposition (SED) of M J/kg. Highlighted inversion pulses: C1 (red), C2 (green), C5 (magenta). Subject automated classifications: #1 in C1, #2 in C5, #3 in full population (closest cluster C2), and #4 in C2. Significant improvements were observed in smaller head shapes, where population-specific pulses effectively recovered signal around sinuses.

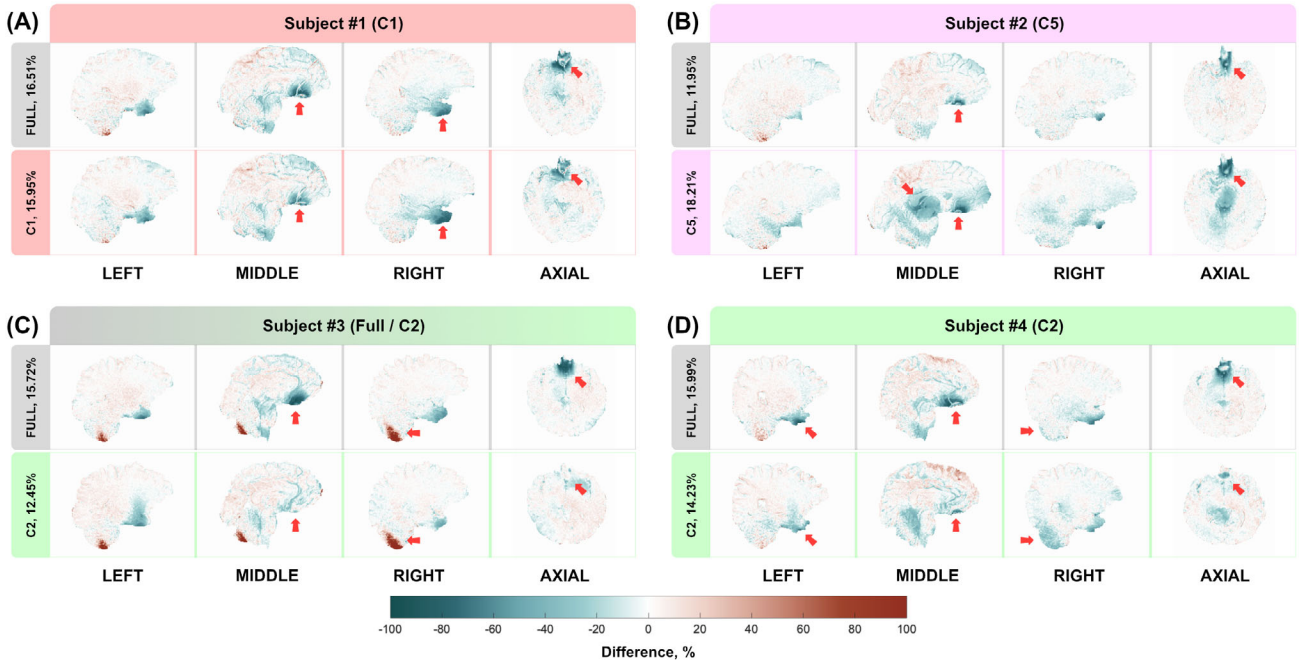

FIGURE 6 Relative difference in T1 values compared to the reference HS4 adiabatic inversion for subjects #1-4 (A-D). "N, M" indicates a pulse designed for cluster N with NRMSE of M across T1 values. Highlighted inversion pulses: C1 (red), C2 (green), and C5 (magenta). Subject automated classifications: #1 in C1, #2 in C5, #3 in full population (closest cluster C2), and #4 in C2.

techniques could be used. Specifically, advanced field mapping methodologies such as actual flip-angle imaging (AFI)[29] and dual refocusing echo acquisition mode (DREAM)[30] have the potential to enhance the accuracy of field maps.

The energy deposition can be managed as a trade-off with performance, leading to a more energy-efficient solution by changing the maximum allowed SED. In our SED unlimited case, the least efficient population-specific pulse exhibited an energy deposition three times lower than the HS4 adiabatic inversion pulse used in the product version of the MP2RAGE sequence.

As previously reported in our *in silico* feasibility study,[15] subpopulations showed the highest performance gains in challenging head shapes in the tails of the population distribution. The dataset analyzed in this study included 39 subjects, which may only represent part of the population. Nonetheless, the head shape metrics (means and standard deviations) aligned with previously reported values.[16] The clusters themselves cannot be very narrow, as the localizer scan's resolution constrains the head measurements' accuracy. The clusters should be sufficiently large to encompass the anatomical variability within the population yet small enough to yield a performance gain.

The automated Python pipeline, integrated within the FIRE framework, demonstrated high repeatability with a minimal standard deviation of 0.1 mm. The observed output variance across multiple executions of identical registrations can be attributed to random sampling and floating-point precision errors. While seeding the registration algorithm can produce fully reproducible measurements, this approach does not inherently enhance the accuracy of the measurements. Therefore, we avoided seeding the registration algorithm.

The current FIRE pipeline implementation provides a flexible sequence-agnostic solution, provided the pulse under consideration has fixed parameters and can be precomputed. It allows defining of any number of clusters by setting maximum acceptable distances to their centers in a configuration file. The algorithm selects the closest cluster within the specified limit. In cases where no such cluster is identified, it defaults to a generic solution that has to be provided in the configuration file. This approach allows the pipeline to be easily customized for different applications and pulse sequences as needed.

The proposed approach is essentially calibration-free, needing only the real-time analysis of the participant's head shape. Routine localizer scans performed during the planning phase can effectively support this process without increasing the total examination time. The analysis takes approximately 10 seconds to measure the relevant parameters and select an appropriate solution, ensuring that the integration of this methodology into clinical workflows remains seamless and does not introduce significant delays.

Upon examining the cluster compositions, we observed that participants with larger head shapes were predominantly male, whereas those with smaller head shapes were mostly female. Although volunteer selection was entirely random, we believe this separation arose naturally in a relatively small dataset. Consequently, one might argue that relying solely on head breadth (HB), head length (HL), and Y-shift as clustering criteria appears limited for improving B_+^1 homogeneity. Nonetheless, our choice to focus on objective head shape measurements derived from standard localizer scans was deliberate. By doing so, we avoided the ethical and practical challenges associated with incorporating demographic variables such as ethnicity or sex. Those factors would require much larger and more diverse datasets. Furthermore, we acknowledge the potential benefits of integrating additional head shape metrics such as Z-shift, for example, and intend to explore these in future studies to improve the clustering process.

Special consideration must be given to cases involving excessive hair volume or cushioning. In our experiments, Subject #4 had an unusually high Y-shift value within the coil due to a substantial hair volume. Despite this, the C2 subpopulation pulse performance remained unaffected. Nevertheless, these edge cases require further investigation to understand and fully address their potential challenges.

5 | CONCLUSION

Segmenting the population into subgroups based on head shape and position can enhance the performance of one-size-fits-all universal inversion pulses in the MP2RAGE sequence for 7T brain imaging. Population-specific pulses, facilitated by the automated pulse selection pipeline, demonstrated improved B_+^1 homogeneity, particularly in smaller head shapes, and reduced energy deposition compared to adiabatic inversion without increasing scan time. Although population-specific pulses did not match the performance of adiabatic inversion pulses, they offer a practical compromise between calibration-free UPs and subject-specific online pTx pulse design.

ACKNOWLEDGEMENTS

The authors acknowledge the facilities and scientific and technical assistance of the National Imaging Facility, a National Collaborative Research Infrastructure Strategy (NCRIS) capability, at the Melbourne Brain Centre Imaging Unit, University of Melbourne. The authors would also like to acknowledge Tobias Kober and Tom

Hilbert for providing the MP2RAGE research application sequence used in this study. Open access publishing facilitated by The University of Melbourne, as part of the Wiley - The University of Melbourne agreement via the Council of Australian University Librarians.

CONFLICTS OF INTEREST

Simon Lévy, Kelvin Chow and Patrick Liebig are employees of Siemens Healthcare.

ORCID

Igor Tyshchenko https://orcid.org/0000-0002-7829-7372
Simon Lévy https://orcid.org/0000-0002-6492-2990
Joseph J. Bartlett https://orcid.org/0000-0003-0684-088X
Bahman Tahayori https://orcid.org/0000-0002-4927-0023
Yasmin Blunck https://orcid.org/0000-0003-3600-9958
Tudor V. Sava https://orcid.org/0009-0009-7917-8170
Kelvin Chow https://orcid.org/0000-0003-0698-1746
Patrick Liebig https://orcid.org/0000-0001-7342-3715
Rebecca Glarin https://orcid.org/0000-0003-0343-8537
Leigh A. Johnston https://orcid.org/0000-0002-5032-4674

REFERENCES

1. Uğurbil K. Imaging at ultrahigh magnetic fields: history, challenges, and solutions. *Neuroimage*. 2018;168:7-32.
2. Ladd ME, Bachert P, Meyerspeer M, et al. Pros and cons of ultra-high-field MRI/MRS for human application. *Prog Nuclear Magn Reson Spectrosc*. 2018;109:1-50.
3. Vaughan JT, Garwood M, Collins CM, et al. 7T vs. 4T: RF power, homogeneity, and signal-to-noise comparison in head images. *Magn Reson Med*. 2001;46:24-30.
4. Wang Z, Lin JC, Mao W, Liu W, Smith MB, Collins CM. SAR and temperature: simulations and comparison to regulatory limits for MRI. *J Magn Reson Imaging*. 2007;26:437-441.
5. Brink JS. Thermal effects associated with RF exposures in diagnostic MRI: overview of existing and emerging concepts of protection. *Concepts Magn Reson Part B*. 2019;2019:1-17.
6. Fiedler TM, Ladd ME, Bitz AK. SAR simulations & safety. *Neuroimage*. 2018;168:33-58.
7. Tannus A, Garwood M. Adiabatic radiofrequency pulse design by composite pulses. *Magn Reson Med*. 1997;10:423-434.
8. Cloos MA, Boulant N, Luong M, et al. Parallel-transmission-enabled magnetization-prepared rapid gradient-echo T1-weighted imaging of the human brain at 7T. *Neuroimage*. 2012;62:2140-2150.
9. Deniz CM, Alon L, Brown R, Zhu Y. Subject- and resource-specific monitoring and proactive management of parallel radiofrequency transmission. *Magn Reson Med*. 2016;76:20-31.
10. Gras V, Vignaud A, Amadon A, Le Bihan D, Boulant N. Universal pulses: a new concept for calibration-free parallel transmission. *Magn Reson Med*. 2017;77:635-643.
11. Gras V, Mauconduit F, Vignaud A, et al. Design of universal parallel-transmit refocusing kT-point pulses and application to 3D T2-weighted imaging at 7T. *Magn Reson Med*. 2018;80:53-65.
12. Le Ster C, Mauconduit F, Massire A, Boulant N, Gras V. Standardized universal pulse: a fast RF calibration approach to improve flip angle accuracy in parallel transmission. *Magn Reson Med*. 2022;87:2839-2850.
13. Herrler J, Liebig P, Gumbrecht R, et al. Fast online-customized (FOCUS) parallel transmission pulses: a combination of universal pulses and individual optimization. *Magn Reson Med*. 2021;85:3140-3153.
14. Herrler J, Heidemann RM, Majewski K, et al. Scalable fast online-customized (FOCUS) pTx pulses for 3D TSE sequences at 7T. *Paper presented at: Proceedings of the 2024 ISMRM & ISMRT Annual Meeting & Exhibition*, Singapore; 2024:4097. https://onlinelibrary.wiley.com/doi/full/10.1002/mrm.29884
15. Tyshchenko I, Lévy S, Jin J, Tahayori B, Blunck Y, Johnston LA. What can we gain from subpopulation universal pulses? A simulation-based study. *Magn Reson Med*. 2024;91:570-582.
16. Ball R, Shu C, Xi P, Rioux M, Luximon Y, Molenbroek J. A comparison between Chinese and Caucasian head shapes. *Appl Ergon*. 2010;41:832-839.
17. Cloos MA, Boulant N, Luong M, et al. kT-points: short three-dimensional tailored RF pulses for flip-angle homogenization over an extended volume. *Magn Reson Med*. 2012;67:72-80.
18. Setsompop K, Wald LL, Alagappan V, Gagoski BA, Adalsteinsson E. Magnitude least squares optimization for parallel radio frequency excitation design demonstrated at 7 tesla with eight channels. *Magn Reson Med*. 2008;59:908-915.
19. Hoyos-Idrobo A, Weiss P, Massire A, Amadon A, Boulant N. On variant strategies to solve the magnitude least squares optimization problem in parallel transmission pulse design and under strict SAR and power constraints. *IEEE Trans Med Imaging*. 2014;33:739-748.
20. Gras V, Luong M, Amadon A, Boulant N. Joint design of kT-points trajectories and RF pulses under explicit SAR and power constraints in the large flip angle regime. *J Magn Reson*. 2015;261:181-189.
21. Jenkinson M, Beckmann CF, Behrens TEJ, Woolrich MW, Smith SM. FSL. *Neuroimage*. 2012;62:782-790.
22. Chow K, Kellman P, Xue H. Prototyping image reconstruction and analysis with FIRE. *Proceedings SCMR 24th Annual Scientific Sessions*. Virtual Meeting; 2008.
23. Fautz HP, Vogel M, Gross P, Kerr A, Zhu Y. B1 mapping of coil arrays for parallel transmission. *Proceedings of the 16th Annual Meeting of ISMRM*; 2008:1247. https://cds.ismrm.org/protected/08MProceedings/PDFfiles/01247.pdf
24. Jezzard P, Balaban RS. Correction for geometric distortion in echo planar images from B0 field variations. *Magn Reson Med*. 1995;34:65-73.
25. Marques JP, Kober T, Krueger G, Zwaag W, Moortele PF, Gruetter R. MP2RAGE, a self bias-field corrected sequence for improved segmentation and T1-mapping at high field. *Neuroimage*. 2010;49:1271-1281.
26. Tustison NJ, Avants BB, Cook PA, et al. N4ITK: improved N3 bias correction. *IEEE Trans Med Imaging*. 2010;29:1310-1320.
27. Avants BB, Tustison NJ, Song G, Cook PA, Klein A, Gee JC. A reproducible evaluation of ANTs similarity metric performance in brain image registration. *Neuroimage*. 2011;54:2033-2044.
28. Henschel L, Conjeti S, Estrada S, Diers K, Fischl B, Reuter M. FastSurfer - a fast and accurate deep learning based neuroimaging pipeline. *Neuroimage*. 2020;219:117012.

29. Yarnykh VL. Actual flip-angle imaging in the pulsed steady state: a method for rapid three-dimensional mapping of the transmitted radiofrequency field. *Magn Reson Med*. 2007;57:192-200.
30. Ehses P, Brenner D, Stirnberg R, Pracht ED, Stöcker T. Whole-brain B1-mapping using three-dimensional DREAM. *Magn Reson Med*. 2019;82:924-934.

SUPPORTING INFORMATION

Additional supporting information may be found in the online version of the article at the publisher's website.

Table S1. Summary of volunteer demographics and physical characteristics. Both B_0 and B_1^+ maps were included in the pulse design.

Figure S1. Visualization showing the intersection (red line) of the midsagittal plane with the target slice identified by the automated measurement pipeline across 39 subjects in the dataset. The red line was expected to be aligned with the anterior commissure - posterior commissure (AC-PC) line.

How to cite this article: Tyshchenko I, Lévy S, Bartlett JJ, et al. In vivo evaluation of population-specific inversion pulses in parallel transmission. *Magn Reson Med*. 2025;94:1878-1888. doi: 10.1002/mrm.30593